Rank-order and morphological enhancement of image details with an optoelectronic processor

Tomasz Szoplik, Javier Garcia, and Carlos Ferreira

In all-optical processors, enhancement of image details is the result of high-pass filtering. We describe an optoelectronic processor in which detail enhancement results from the digitally calculated difference between an original input image and its low-pass filtered version. The low-pass filtering is realized through the rank-order median and the morphological opening and closing operations calculated by use of the optical convolver. It is shown that the normalized difference between the morphological white and black top hats enhances bright and dark image details analogously to the rank-order unsharp masking.

Key words: Optoelectronic image processing, optoelectronic image enhancement, rank-order filters, morphological filters.

1. Introduction

Two important methods of nonlinear image processing are rank-order[1–4] and morphological[5–7] filtering. Though different from the point of view of mathematical approach, they may lead to similar image modifications. It was proven that rank-order filters are equivalent to those morphological filters that commute with thresholding.[8,9] This condition is met for the cases of set- and function-processing (i.e., binary and gray-scale image-processing) morphological filters that involve a binary structuring element (that is, a flat kernel of local convolution). Thus rank-order and morphological filtering can be performed in linear optical systems complemented with electronics, which adds nonlinear thresholding to the optical convolution. In both methods, processing of a gray-scale image slice by slice is based on the threshold decomposition concept,[1] which led to the definition of the stacking property[2] of Boolean functions (operators). Nonlinear image processing based on the thresholded local convolution approach permits operations on image details of the size smaller than or equal to that of the convolution kernel. The processing results in modifications of local histograms calculated for neighborhoods contained within the kernel windows. The purpose of local histogram modifications can be various, examples of which are noise removal, image detail enhancement, skeletonization, and segmentation. In both rank-order and morphological processing the mechanism of detail enhancement is quite similar. The details are extracted as the difference (residue) between the original image and its nonlinearly processed versions, which are low-pass filtered. In rank-order processing the usual low-pass filter is the median one, which neglects extreme image pixel values contained within the local convolution window. In morphological processing the opening and closing transformations have selective low-pass filter properties. In binary images the opening filters out small sets and small convex details of objects. Thus the gray-scale images are smoothed by the opening owing to removal of convex details that on each grade of gray are thinner than the structuring element. The morphological closing operation is dual to the opening. Therefore in binary images the closing fills in small dark holes within objects and connects closely disjointed parts of objects into one. The gray-scale images are smoothed by the closing owing to removal of concave details that are smaller than the kernel. In terms of intensity the opening removes bright details of an image, while the closing removes dark details. Low-pass filtering is easily performed in an optical system because of its limited modulation transfer function. Thus the efficiency of optical systems in low-pass filtering results in good performance of hybrid high-pass filtering processors. In both methods the size and the shape

When this research was performed, the authors were with the Departamento Interuniversitario de Optica, Universitat de Valencia, Burjassot 46100, Spain. T. Szoplik's permanent address is the Instytut Geofizyki, Universytet Warszawski, Pasteura 7, Warszawa 02-093, Poland.

Received 7 December 1993; revised manuscript received 25 July 1994.

0003-6935/95/020267-09$06.00/0.

of preserved details depend on the neighborhoods within which the operations are realized.

There are several optoelectronic implementations of morphological and rank-order nonlinear processors.[10–19] In all of them, because of optical convolution, the digital computations are reduced to calculating the maximum, minimum, and other rank-order values and depend less on the neighborhood shape and size. In the first demonstration of the optoelectronic rank-order processor a binary spatial light modulator (SLM) was employed to introduce simultaneously into an optical convolver all of the binary slices of an input image.[10] A computer-generated hologram played a double role of an image beam deflector for slices and a structuring element. In this experiment a gray-scale image of 48×48 pixels with 16 gray levels was processed in real time. In another hybrid morphological processor the real-time programmable processing of limited-size images was presented.[12] A binary input image and a structuring element were introduced into an optical system by means of two SLM's. The use of a lenslet array illuminator yielded a convolution due to angular projection. The convolution with angular projection was also employed in the morphological processor with a laser beam scanner.[14] In the morphological processor based on a coherent 4-f type correlator the impulse response of the Fourier-plane holographic filter played the role of a structuring element.[15,16] In other realizations of rank-order and morphological processors, noncoherent convolvers by use of either a plane of misfocus or shadow casting were applied.[11,17–19] The slices of the gray-scale input images were introduced into the convolvers by means of photographic transparencies, a TV monitor, or an SLM. In all of the above-mentioned systems, looping and sequential regime of work were necessary as a consequence of the sequential structure of rank-order and morphological filters on the one hand and the threshold decomposition concept and stacking property on the other.

Recently Tasto and Rhodes showed that both rank-order and morphological filtering of threshold decomposed images realized in optoelectronic processors exhibits a high degree of noise immunity and permits high-accuracy processing.[20] Their assessment as well as the progress in real-time processing techniques encourages continuation of research on hybrid optoelectronic systems for both rank-order and morphological processing.

Our aim here is to demonstrate the feasibility and quality of optoelectronic experimental results of three algorithms for enhancement of image details: rank-order unsharp masking and morphological black and white top hats. To establish a link between unsharp masking and morphological top hats, we define the normalized difference between white and black top hats. The difference algorithm enhances both bright and dark details. The experiment is done on a realistic-size image with rich texture.

2. Rank-Order and Morphological Algorithms for Enhancement of Image Details

Rank-order and morphological methods of image improvement can be divided into two broad groups of algorithms, which aim at either image smoothing or enhancement of image details.[3–7,18,21] Image-smoothing algorithms are used for removal of noise that has one of several possible properties or that is a mixture of different types of noise. At the same time, information about fine image details is preserved. The noise-suppression algorithms are used for preprocessing of images that afterward are subjects of enhancement operations such as, for instance, histogram modifications or edge extraction. A sequence of proper operations may lead to a considerable image improvement appreciated by a human observer. Application of smoothing and enhancing algorithms may also precede pattern-recognition tasks.

A. Rank-Order Algorithms for Enhancement of Image Details

Let $\{V(\mathbf{k})\}$ be a discrete input image with Q gray-scale levels of intensity quantization: $\mathbf{k} = (k_1, k_2)$ is a vector coordinate of an input image element; $k_1 = 1, \ldots, N_1$ and $k_2 = 1, \ldots, N_2$; $N_1 \times N_2 = N$ is the image matrix size. According to the threshold decomposition concept,[1] the $\mathbf{k}$th element $V(\mathbf{k})$ of an input image is represented as a sum of $\mathbf{k}$th elements of all binary slices as

$$V(\mathbf{k}) = \sum_{q=1}^{Q-1} X_q(\mathbf{k}), \qquad (1)$$

where $X_q(\mathbf{k})$ is the $\mathbf{k}$th element of a binary slice of an input image obtained through decomposition with a threshold q; that is,

$$X_q(\mathbf{k}) = \begin{cases} 1 & \text{if } V(\mathbf{k}) \geq q \\ 0 & \text{otherwise} \end{cases}.$$

For each slice $\{X_q(\mathbf{k})\}$, where braces denote the whole set of q-level elements, local operations are performed within a spatial neighborhood S of arbitrary size and shape that is similar for each $\mathbf{k}$th input-image element. The spatial neighborhood S is cast by a scanning binary (flat) structuring element that characterizes the local convolution. The local-convolution operation can be very efficiently performed in a computer unless the structuring elements do not become too large. Alternatively, local convolutions can be accomplished in parallel in optical correlators. We believe that fully programmable correlators for processing of large images by means of large and arbitrarily shaped structuring elements should become feasible soon.

The possibility of parallel optical calculation of local convolutions was the basis of a recently proposed optical–digital method of local histogram calculation.[17] This method results from a theorem proved in Ref. 17, which says that the local q-level histogram of an arbitrary neighborhood in an input image is equal to the pointwise difference of the two convolution patterns obtained by convolving the slices at the levels $q + 1$ and q with a binary mask, thereby defining the neighborhood. We note that, for each pixel of the input image, the pixel value in the convolution pattern of the q-level binary slice and the kernel is equal to the number of pixels in the neighborhood that are on the q-level and higher values.

Detail-enhancing algorithms are designed to increase local nonhomogeneities of intensity distribution of an input image. An increase of local contrast can be accomplished in a variety of ways. A simple and linear method is to enhance these pixels that differ from average pixel values calculated within its spatial neighborhoods S:

$$Y(\mathbf{k}) = \mathrm{mean}\{S[V(\mathbf{k})]\} + G(V(\mathbf{k}) - \mathrm{mean}\{S[V(\mathbf{k})]\}), \tag{2}$$

where the output pixel value $Y(\mathbf{k})$ is given by the sum of a bias term equal to the average pixel value calculated within neighborhood S of the input pixel $V(\mathbf{k})$ and another term that is a difference between the input pixel value and the before-mentioned average enhanced by a gain coefficient G. The above algorithm becomes nonlinear when the mean operation is replaced with the med operation; that is, the median value of the neighborhood S is considered as a reference.

The most general nonlinear rank-order unsharp masking algorithm (UM) is defined as follows[22]:

$$\mathrm{UM}[V(\mathbf{k})] = \mathrm{A} + G(V(\mathbf{k}) - \mathrm{med}\{S[V(\mathbf{k})]\}), \tag{3}$$

where $S[V(\mathbf{k})]$ is an arbitrary neighborhood of the $\mathbf{k}$th element of an input image, A is the offset, G is the gain coefficient of input-image details that differ from the median value, and minus denotes a pointwise subtraction. Taking advantage of the threshold decomposition concept, we process in sequence binary slices $\{X_q(\mathbf{k})\}$ of the input image rather than the gray-scale input image $\{V(\mathbf{k})\}$ itself. For each $\mathbf{k}$th input slice element a local convolution is made and the median value $\mathrm{med}\{S[X_q(\mathbf{k})]\}$ is calculated within the $\mathbf{k}$th-element neighborhood, S, defined by the binary convolution kernel. The pointwise sum of all processed slices gives the output gray-scale image. Coefficients A and G are image dependent and are calculated as follows. Pointwise subtracting the median from the original, we find minimum $(-n)$ and maximum (m) difference pixel values as well as the zero level (as a fraction f of the full range $[-n, m]$). Then the gain coefficient is calculated as $G = 255/(m + n)$ and the offset $A = 255f$.

B. Morphological Algorithms for Enhancement of Image Details

Morphological filters are composed of two basic operations: erosion and dilation. The erosion is defined as the locus of the center of the structuring element S when S is included in the binary slice X, such that in the extreme case it follows the border tangentially from inside. The dilation is defined as the locus of the center of the structuring element when S intersects X, such that in the extreme case it follows the border tangentially from outside. The simplest morphological filters are the opening and closing. The morphological opening is defined as follows:

$$\gamma_S\{X_q(\mathbf{k})\} = \delta_S\epsilon_S\{X_q(\mathbf{k})\}, \tag{4}$$

where the erosion ϵ_S of the image slice $\{Xq(\mathbf{k})\}$ by the structuring element S is followed by the dilation δ_S of the looped eroded slice by the same kernel. The opening filters out bright details of an input image and is frequently used to remove salt elements of the two-sided impulsive noise. The opening of a gray-scale image $\gamma_S\{V(\mathbf{k})\}$ is obtained by stacking of the processed binary slices. The morphological white-top-hat algorithm (WTH), which enhances bright details, is defined as the difference (residue) between the input image and its opening[23]:

$$\mathrm{WTH}\{V(\mathbf{k})\} = \{V(\mathbf{k})\} - \gamma_S\{V(\mathbf{k})\}, \tag{5}$$

where minus denotes pointwise subtraction, which results in a positive representation of high-intensity details.

In the black-top-hat algorithm (BTH) the morphological closing is employed. This operation, dual to opening, is defined as

$$\varphi_S\{X(\mathbf{k})\} = \epsilon_S\delta_S\{X(\mathbf{k})\}, \tag{6}$$

where dilation and erosion are made in reverse order to that of the opening. The closing filters out dark details of an input image and is frequently used to remove pepper elements of the two-sided impulsive noise. Here also the closing of a gray-scale image $\varphi_S\{V(\mathbf{k})\}$ results from summing up the processed binary slices. The morphological black-top-hat algorithm, which enhances dark features, is defined[23] as

$$\mathrm{BTH}\{V(\mathbf{k})\} = \varphi_B\{V(\mathbf{k})\} - \{V(\mathbf{k})\}, \tag{7}$$

where minus denotes pointwise subtraction of an original from its closing, which results in a negative representation of low-intensity details.

For the purpose of comparison of results of rank-order and morphological methods for image detail enhancement we propose to combine white and black top hats. The aim is to unite bright and dark details obtained with top hats, as in the case of unsharp masking. The difference $D\{V(\mathbf{k})\}$ between white and black top hats, which retrieves the original contrast of details, is defined as follows:

$$D\{V(\mathbf{k})\} = A + G[\mathrm{WTH}\{V(\mathbf{k})\} - \mathrm{BTH}\{V(\mathbf{k})\}], \tag{8}$$

where A is a normalization constant and G is the gain coefficient of extracted details, both of which are calculated similarly as in the case of Eq. (3). Analogy between the unsharp masking and the difference of top-hats algorithms is straightforward. In the first one, bright and dark details that outlie from the local median values are properly increased by a factor of G

and displayed on a bias level A calculated for the whole image. In the second one, bright and dark details are obtained from calculated differences between the input image and its morphological opening and closing, then are multiplied by the gain coefficient G, which depends on the dynamic range of the difference of top hats, and the details are displayed on a bias level A calculated for the whole image. Both algorithms are very good contrast detectors suitable for enhancement of bright and dark details that are smaller than or equal in size and shape to the structuring element used to modify the input image.

3. Experiment and Results

A. Characteristic of an Optoelectronic Experiment Using Thresholded Convolution

Let us discuss a few sources of noise usually present in optoelectronic processors composed of one or two SLM's, which introduce an input image and a structuring element into the system, a CCD camera, and a frame grabber. Frequently, an input image is introduced into the optical convolver by means of an SLM in the form of a liquid-crystal display (LCD). Because of nonuniform thickness of the liquid-crystal sandwich and nonuniform illumination, the intensity values corresponding to logic ones and zeros vary from one element to another at random for both. For LCD pixels the contrast ratio C is defined as

$$C = I_{\max}/I_{\min}, \tag{9}$$

where $I_{\max}$ and $I_{\min}$ are the intensities transmitted by LCD pixels that are on and off. According to Ref. 24 the minimum contrast ratio for each pixel of the Epson VP-100PS-type LCD used in our experiment is 40. According to Laude *et al.*,[25] the corresponding maximum contrast ratio for the white-light illumination reaches 60. We want to have an image input device with as a high contrast ratio as possible. If it is equal to k, then for a slice that has k times more pixels in the zero level than in the one level, the background contains the same amount of energy as the foreground. A limited value of the contrast ratio results in a high background level; therefore proper adjustment of offset and gain in the frame grabber is necessary to optimize the dynamic range of recorded images.

At present the best low-end LCD that is commercially available does not exceed 480×440 pixels in size and has a contrast ratio on the level of 100:1. In fully programmable optical convolvers it can be used for introduction of large structuring elements of arbitrary shape. The recent development of vertical-cavity surface-emitting lasers gives hope that, in the near future, microlaser arrays can be used as image input devices in optical convolvers. Nowadays vertical-cavity surface-emitting laser arrays are easily switched from the fully on to the fully off state with frequencies lower than 100 MHz.[26]

If a structuring element is introduced into the system by means of an SLM, the threshold level depends also on the number of pixels in the kernel. The bigger the structuring element, the higher the threshold.[12] Recent analysis of noise effects in optoelectronic order-statistics filtering concludes that operations using higher thresholds have higher probabilities of error.[20] Consequently, instead of erosion, it is advisable to make a binary logic inversion of a slice, calculate dilation, and again make a complement. In principle, the idea is correct. However, in the case of realistic-size images with full gray scale and rich texture it should be used cautiously. In such images the first slice is mostly composed of ones and the last one of zeros. Thus routine use of the above method of complement processing with respect to all of the slices makes no sense. With the same method one cannot improve the results of processing the first and the last slices. There is a possibility of using the method in an image-dependent way, in which case the contrast ratio of the SLM's used should be taken into account. In our experiment, dilations, medians, and erosions are calculated directly.

For the past 20 years LCD's have been produced in thin-film-transistor technology.[27] In this technology each pixel of a LCD array has a thin-film transistor that permits active addressing. The transistor gate is attached to a horizontal row electrode, the drain is attached to a vertical column electrode, and the source is attached to the liquid-crystal electrode. The pixel array is activated a row at a time by activating the gate lines. In principle this technology ensures accurate switching on and off of individual pixels. Because of cross talk, however, some of the pixels may switch to another state. Let us consider possible consequences on the example of the image of a wedge with uniform distribution of shade, composed of 256×256 pixels, and having 256 gray-scale levels. For such an image the difference in the population of ones between two subsequent slices is 256, that is, 0.004 of the total number of pixels. For an arbitrary image, such a difference can be even smaller. The cross talk may disturb this small difference considerably. We conclude that, for our purpose, low-pass filtering in an optoelectronic convolver, the limitation of the number of gray-scale levels is justified and advisable. The use of 16 gray-scale levels of the original picture instead of all 256 ensures that the number of zeros in subsequent slices does not decrease when threshold q increases. In this way, cross talk increases the level of noise, but it does not cause inversion of the population of ones in a sequence of slices.

In an optoelectronic system composed of a liquid-crystal SLM, a CCD camera, and a frame grabber, there are two more sources of noise, which enter the information channel. First, the analog signals are resampled three times with different resolutions on their loop between the frame grabber, the SLM, and the CCD camera. Second, the random noise of the CCD camera and the SLM reduces the dynamic range of convolution patterns.

The morphological opening and closing given with

Eqs. (3) and (5) employ thresholds on minimum (dilation) and maximum (erosion) levels, which in digital processing correspond to 0 and 255 levels, respectively. In optoelectronic implementations the minimum and maximum threshold levels are located just above and below the levels of noise, which comes from the above-mentioned sources. For each pixel of the input image the pixel value in the convolution pattern of the q-level binary slice and the kernel is equal to the number of pixels in the neighborhood that are at the q level value and higher. To find the threshold levels, we use the theorem on local histogram calculation,[17] which was recalled in Section 2. In principle, both local and global histograms, which are functions of the q argument, should be nondecreasing for zeros and nonincreasing for ones. The existence of noise, however, may cause small discrepancies between theory and practice, especially for extreme q levels.

B. Experimental System

In our experiment an optoelectronic morphological image processor with feedback was used, which was a modified version of that described in a previous paper.[19] Figure 1 shows a block diagram of the processor. An input gray-scale image is digitally threshold decomposed into a stack of binary slices. The next operation is performed in the optical white-light convolver with a plane of misfocus. Binary slices are displayed in time sequence on the Epson VP-100PS-type LCD and imaged with a camera lens onto the Pulnix TM-765 CCD camera. The system point-spread function is controlled by misfocusing and the use of a diaphragm. The point-spread function plays the role of a structuring element. In this manner every binary slice is optically convolved with a binary convolution kernel, which results in a stack of gray-scale convolution patterns. Convolution patterns recorded by the CCD camera are sent to the Matrox PIP-1024B video digitizer board. After proper thresholding in the frame grabber, the following pointwise operations on the binary convolution patterns and further processing are made on a microcomputer. In the case of morphological filters, results of intermediate operations are reintroduced into the LCD as looped inputs. The processor is equipped with TV monitors for observation of input slices, recorded convolution patterns, thresholded convolution patterns, and final results.

The white-light convolver with a plane of misfocus is one of the few possible convolver configurations. The others are angular projection convolvers and shadow-casting correlators.[28] Frequent use of white-light convolvers in morphological processors and optical parallel logic processors with shadowgrams has triggered recent interest in their performance.[29,30]

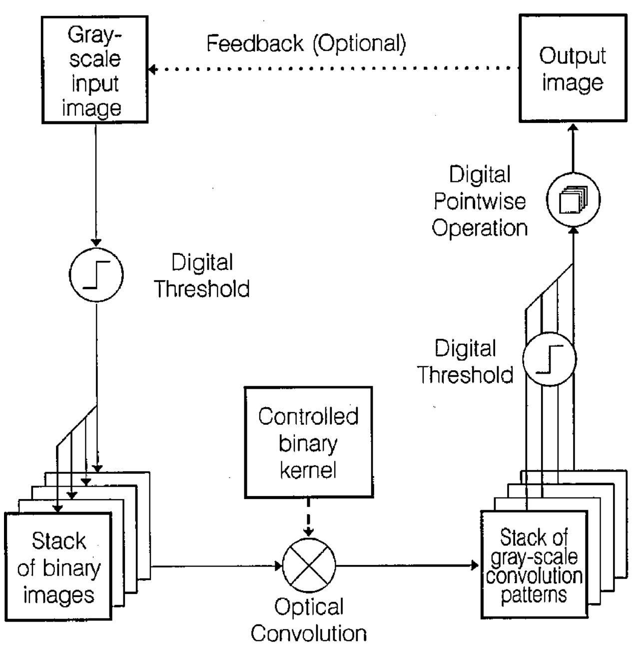

Fig. 1. Block diagram of the morphological optoelectronic image processor. Operations are shown in circles, and data arrays are shown in squares.

C. Comparison of Experimental Optical Results and Digital Results

Performance of detail-enhancement algorithms is demonstrated on the input image of 256×256 pixels and 16 gray levels, which is shown in Fig. 2(a). Figure 2(b) presents the results of a digital median filter with a binary kernel of 5×5 pixels. Figure 2(c) shows an example of the output of an optical median filter with a flat structuring element of the same size. Visual examination of both results confirms good performance of the optoelectronic processor. For the purpose of quantitative comparison we use the mean absolute error (MAE) as a measure of similarity. The MAE, which is frequently used in filter optimization problems,[31] is defined as follows:

$$\mathrm{MAE} = \frac{1}{N} \sum_k |\mathrm{med}_\mathrm{d}\{S[V(\mathbf{k})]\} - \mathrm{med}_\mathrm{op}\{S[V(\mathbf{k})]\}|, \quad (10)$$

where subscripts d and op indicate digitally and optically calculated medians. The absolute value of the difference (i.e., error) between optical and digital results is summed over the whole image matrix, normalized to the 256 gray-levels score, and divided by the total number of pixels. Analogously, MAE can be defined for morphological operations and filters used in our experiment. Table 1 details values of such experimental parameters as MAE, minimum error, maximum error, and threshold value. In the first row, experimental parameters of optoelectronic calculation of the median are presented. The MAE equals 2.4 ± 0.1 gray-scale levels of the 0–255 range, which means that the optical median filtration is made within 1% accuracy with respect to the digital calculations. For some pixels the maximum difference between optical and digital results reaches almost half of the gray-scale range, however. In principle the threshold value for obtaining the median should be on the level of 0.5. Nevertheless, the

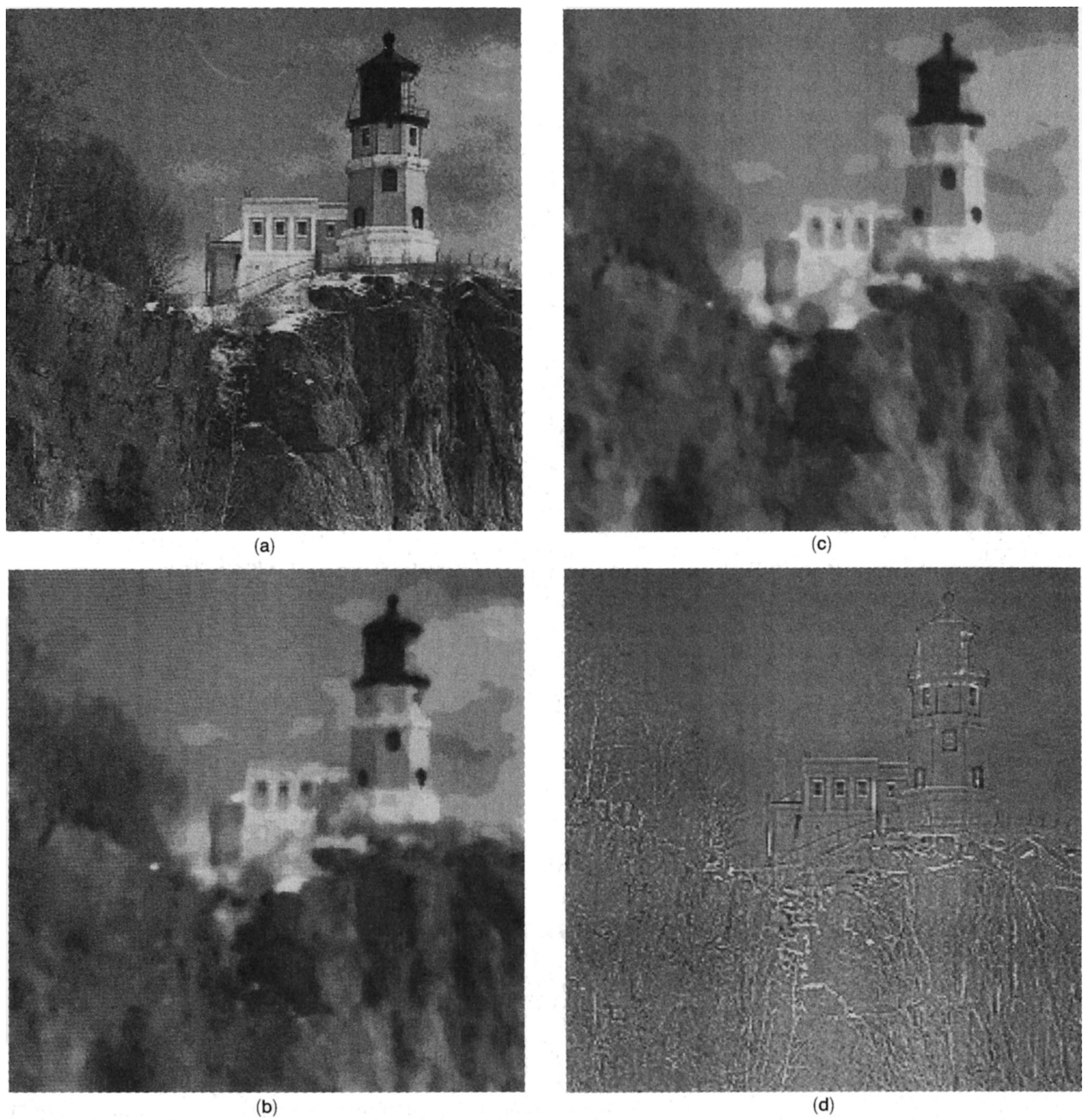

Fig. 2. Experimental results of digital and optoelectronic calculations: (a) input image of 256×256 pixels with 16 gray levels, (b) digital median filtration with a square binary kernel of 5×5 pixels [(c)–(h) are also obtained with a square binary kernel of 5×5 pixels] (c) optical median filtration, (d) digital unsharp masking, (e) optical unsharp masking, (f) optical morphological black top hat, (g) optical morphological white top hat, (h) normalized difference of optical white and black top hats.

above-discussed sources of noise can produce a shifting of the experimental local histograms. Therefore the experimental threshold value is 0.55 ± 0.05. With this threshold value the MAE is minimized.

According to Eq. (2), the results of digital and optical median filtering are used to calculate unsharp masking. Pointwise subtracting the median from the original, we find minimum $(-n)$ and maximum (m) difference pixel values as well as the zero level (as a fraction f of the full range $[-n, m]$). The gain coefficient is calculated as $G = 255/(m + n)$. The offset equals $A = 255f$. In Figs. 2(d) and 2(e) the results of digital and optical unsharp masking are presented, respectively. Obviously they preserve the similarity of digital and optical results of median filtration.

Intermediate optoelectronic operations necessary to obtain morphological white and black top hats are

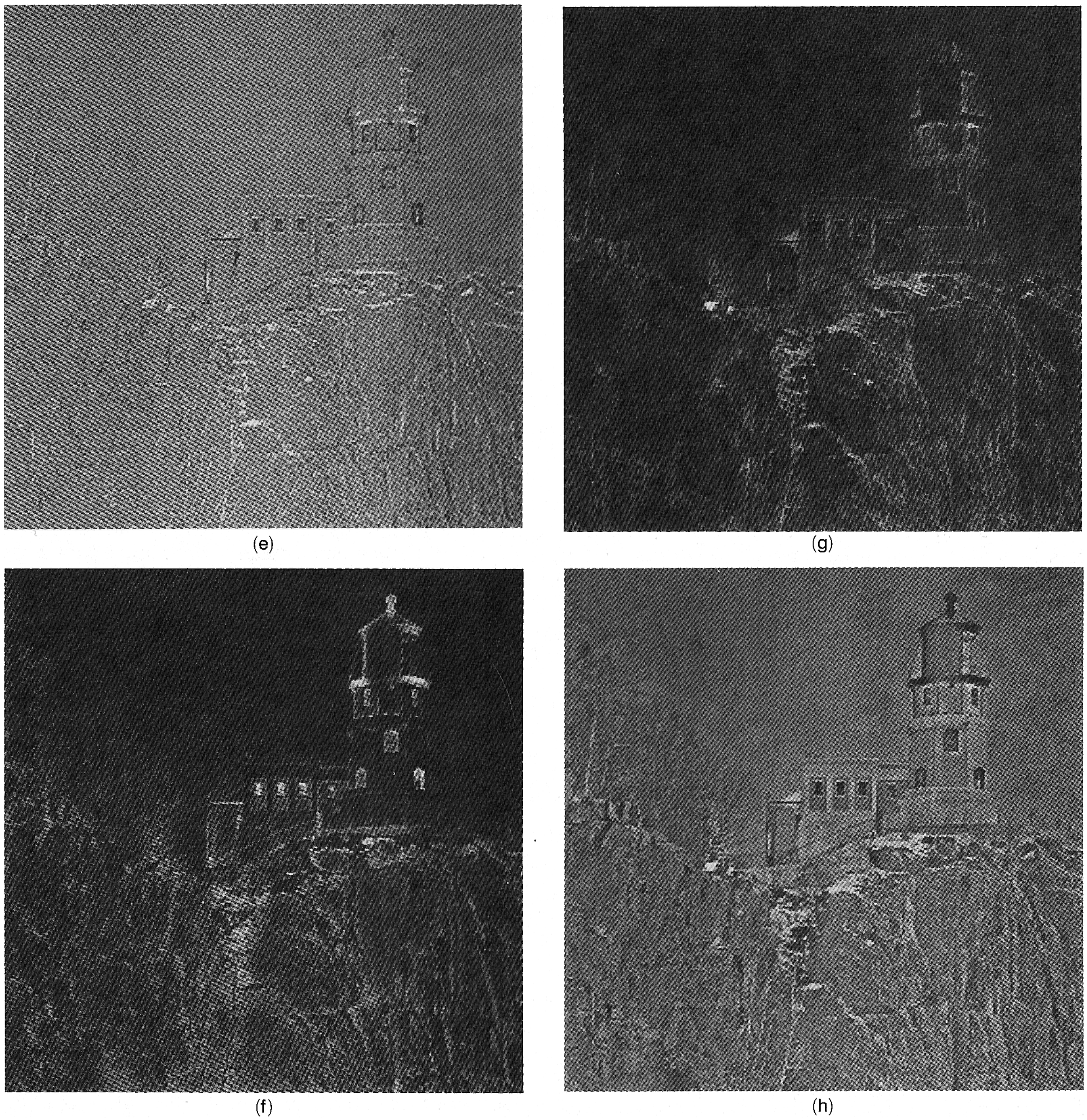

Fig. 2. continued.

summarized in Table 1. The second and the third rows contain experimental parameters of the calculated erosion and dilation. In contrast to theoretical predictions the difference between digital and optical dilations is greater than in the case of the median filter. The accuracy of optical calculation decreases to ~1.6%. For erosion we obtain, in accordance with expectations, the worst result. The accuracy of optical calculation in comparison with the digital one decreases to ~3.2%. The last two rows of Table 1 present parameters of optical calculating of opening and closing, which simultaneously correspond with

Table 1. Values of Experimental Parameters[a]

Filter Type	MAE	min er	max er	th
Median	2.4 ± 0.1	0	104 ± 8	0.55 ± 0.05
Erosion	7.9 ± 0.7	0	160 ± 16	0.975 ± 0.005
Dilation	4.0 ± 0.2	0	144 ± 16	0.025 ± 0.005
Opening	8.0 ± 0.3	0	128 ± 16	0.12 ± 0.03
Closing	6.9 ± 0.1	0	144 ± 16	0.955 ± 0.005

[a]Mean absolute error (MAE), minimum error (min er), maximum error (max er), and threshold value (th) are listed for optoelectronic calculation of the following filters: median, erosion, dilation, opening, and closing.

calculating white and black top hats, respectively. In the case of opening we list parameters of the second operation, that is, of dilation made on the eroded image. The MAE and the minimum and maximum errors have values similar to the case of regular erosion. Thus errors made in two subsequent steps do not accumulate in a direct way. The threshold level of dilation made on the eroded image is 5 times higher than in the case of regular dilation. Finally, for closing, that is, erosion made on the dilated image, we find the experimental parameters comparable to those obtained for the case of regular erosion.

Figures 2(f) and 2(g) show black and white top hats calculated optically according to Eqs. (6) and (4), respectively. We note that both results of morphological processing are satisfactory. The wide presence of a black background confirms the good quality of optically calculated opening and closing.

Figure 2(h) presents the result of the difference between optical white and black top hats calculated according to Eq. (7). The normalization constant A and the gain coefficient G are calculated in exactly the same way as in the case of the unsharp masking algorithm. We note that the experimental morphological result that combines bright and dark details of the image is easier to examine visually than the results of a rank-order unsharp masking algorithm calculated either digitally or optically. It is a consequence of the opening, closing, and median filter definitions that the combination of white and black top hats has a broader histogram than unsharp masking. Thus in the case of the morphological difference of top hats the dynamic range of the output image is more evenly employed than in the unsharp masking case.

4. Concluding Remarks

Optoelectronic implementation of the rank-order and morphological algorithms for image detail enhancement has been presented and compared with digitally calculated results. High-pass morphological and rank-order filtering based on calculation of a residue of an input image and its processed version does not depend strongly on the quality of optically realized low-pass filtering. The optical part of the system is a white-light convolver using the plane of misfocus. The input image is introduced into the system by means of the Epson VP-100PS-type LCD, which is built in thin-film-transistor technology. Owing to cross talk, error in row- and column-wise addressing of pixels may result in that a **k**th pixel value in the upper slice $\{X_{q+1}(\mathbf{k})\}$ being bigger than the same **k**th pixel value in the lower qth slice. Therefore for the purpose of optical low-pass filtering it is advisable to use a limited number of slices, which in consequence are more sparse. In this way the benefits of using an optical convolver are twofold: first, convolutions are made in parallel, and calculation time does not depend on the structuring-element size and shape; second, processing of a fraction of the whole set of 255 slices is sufficient. From the point of view of a human interpreter, however, the quality of results remains good.

The experimental optical results of the median filtering and the morphological erosion, dilation, opening, and closing are compared with the digitally calculated correspondents. The mean absolute error defined by Eq. (9) describes the average per image pixel distance between digitally and optically calculated results. An optical median is calculated within 1% accuracy with respect to the digital calculations. For optical dilation the accuracy decreases to 1.6%. For optically calculated closing, accuracy decreases to 2.7%. The lowest accuracy is found for the cases of optical erosion and opening, only 3.1%.

In this paper we have defined the normalized difference between morphological white and black top hats, which enhances bright and dark details of an input image simultaneously. The experimental result of the difference algorithm is favorably compared with that of the rank-order unsharp masking algorithm, the reason being the better use of the dynamic range of the output image. Both algorithms give image-dependent results; however, probably in most of the cases, the top-hats difference algorithm gives an output image with a bigger number of well-populated gray-scale levels in the histogram than the unsharp masking algorithm. This results from the fact that the top-hat difference algorithm is defined by combination of erosions and dilations, that is, through maximum and minimum thresholds. Consequently, visual inspection of the top-hats difference algorithm output is easier than in the other case, as the overall contrast is higher.

The optoelectronic processor performance depends on the level of noise present in the system. Several sources of noise have been discussed. One of the most important is the limited contrast ratio of the LCD used. Nevertheless, we believe that improvement of the accuracy of optical calculations of rank-order and morphological filters will take place in the near future.

This work was supported by the Spanish project of the Comisión Interministerial de Ciencia y Tecnología (project TAP93-0667-C03-03). T. Szoplik acknowledges a GO WEST grant from the Commission of the European Communities, Cooperation in Science and Technology with Central and Eastern European Countries (grant CIPA3511CT920648). C. Ferreira acknowledges a GO EAST grant from the Commission of the European Communities, Cooperation in Science and Technology with Central and Eastern European Countries (grant ERB-CIPA-CT-93-1671).

References

1. J. P. Fitch, E. J. Coyle, and N. C. Gallagher, Jr., "Median filtering by threshold decomposition," IEEE Trans. Acoust. Speech Signal Process. **ASSP-32,** 1183–1188 (1984).
2. P. D. Wendt, E. J. Coyle, and N. C. Gallagher, Jr., "Stack filters," IEEE Trans. Acoust. Speech Signal Process. **ASSP-34,** 898–911 (1986).

3. V. Kim and L. Yaroslavskii, “Rank algorithms for picture processing,” Comput. Vis. Graph. Image Process. **35,** 234–258 (1986).
4. I. Pitas and A. N. Venetsanopoulos, *Nonlinear Digital Filters. Principles and Applications* (Kluwer, Dordrecht, The Netherlands, 1990), pp. 63–150.
5. J. Serra, *Image Analysis and Mathematical Morphology* (Academic, London, 1982).
6. J. Serra, “Introduction to morphological filters,” in *Image Analysis and Mathematical Morphology. Theoretical Advances*, J. Serra, ed. (Academic, London, 1988), pp. 101–114.
7. E. R. Dougherty and R. P. Loce, “Efficient design strategies for the optimal binary digital morphological filter: probabilities, constraints, and structuring-element libraries,” in *Mathematical Morphology in Image Processing*, E. R. Dougherty, ed. (Dekker, New York, 1993), pp. 43–120.
8. P. Maragos and R. W. Schafer, “Morphological filters. I. Their set-theoretic analysis and relations to linear shift-invariant filters,” “Morphological filters. II. Their relations to median, order-statistics, and stack filters,” IEEE Trans. Acoust. Speech Signal Process. **ASSP-35,** 1153–1184 (1987).
9. P. Maragos, “Tutorial on advances in morphological image processing and analysis,” Opt. Eng. **26,** 623–632 (1987).
10. E. Ochoa, J. P. Allebach, and D. W. Sweeney, “Optical median filtering using threshold decomposition,” Appl. Opt. **26,** 252–260 (1987).
11. J. M. Hereford and W. T. Rhodes, “Nonlinear optical image filtering by time-sequential threshold decomposition,” Opt. Eng. **27,** 274–279 (1988).
12. Y. Li, A. Kostrzewski, D. H. Kim, and G. Eichmann, “Compact parallel real-time programmable optical morphological image processor,” Opt. Lett. **14,** 981–983 (1989).
13. P. Cambon and J.-L. Bougrenet de la Tocknaye, “Mathematical morphology processor using ferroelectric liquid crystal light valves: principle,” Appl. Opt. **28,** 3456–3460 (1989).
14. B. D. Duncan, T.-C. Poon, and R. J. Pieper, “Real-time nonlinear image processing using an active optical scanning technique,” Opt. Laser Technol. **23,** 19–24 (1991).
15. E. Botha, J. Richards, and D. Casasent, “Optical laboratory morphological inspection processor,” Appl. Opt. **28,** 5342–5350 (1989).
16. D. Casasent, R. Schaefer, and R. Sturgill, “Optical hit-miss morphological transform,” Appl. Opt. **31,** 6255–6263 (1992).
17. V. Kober, T. Cichocki, M. Gedziorowski, and T. Szoplik, “Optical-digital method of local histogram calculation by threshold decomposition,” Appl. Opt. **32,** 692–698 (1993).
18. V. Kober, J. Garcia, T. Szoplik, and L. P. Yaroslavsky, “Nonlinear image processing based on optical-digital method of local histogram calculation,” Intl. J. Opt. Comput. **2,** 367–383 (1993).
19. J. Garcia, T. Szoplik, and C. Ferreira, “Optoelectronic morphological image processor,” Opt. Lett. **18,** 1952–1954 (1993).
20. J. L. Tasto and W. T. Rhodes, “Noise immunity of threshold decomposition optoelectronic order-statistic filtering,” Opt. Lett. **18,** 1349–1351 (1993).
21. Y. S. Fong, C. A. Pomalaza-Ráez, and X. H. Wang, “Comparison study of nonlinear filters in image processing applications,” Opt. Eng. **28,** 749–760 (1989).
22. W. F. Schreiber, “Wirephoto quality improvement by unsharp masking,” J. Pattern Recog. **2,** 111–121 (1970).
23. F. Meyer, “Contrast feature extraction,” Pract. Metallogr. **8,** 374–380 (1978).
24. Seiko Epson Corporation, Epson liquid-crystal video projector VP-100PS service manual (Seiko Epson Corporation, Nagano, Japan, 1990).
25. V. Laude, S. Mazé, P. Chavel, and Ph. Réfrégier, “Amplitude and phase coding measurements of a liquid crystal television,” Opt. Commun. **103,** 33–38 (1993).
26. M. Osinski, Center for High Technology Materials, University of New Mexico, Albuquerque, N.M. 87131-6081 (personal communication).
27. W. E. Howard, “Thin-film-transistor/liquid crystal display technology: An introduction,” IBM J. Res. Dev. **36**(1), 3–10 (1992).
28. J. Knopp and M. F. Becker, “Generalized model for noncoherent optical convolvers and correlators,” Appl. Opt. **17,** 984–985 (1978).
29. K. Raj, D. W. Prather, R. A. Athale, and J. N. Mait, “Performance analysis of optical shadow-casting correlators,” Appl. Opt. **32,** 3108–3112 (1993).
30. M. Gedziorowski, T. Szoplik, and C. Ferreira, “Resolution of a lensless shadow casting correlator with partially coherent illumination,” Opt. Commun. **106,** 167–172 (1994).
31. E. J. Coyle and J.-H. Lin, “Stack filters and the mean absolute error criterion,” IEEE Trans. Acoust. Speech Signal Process. **36,** 1244–1254 (1988).